HHS Public Access

Author manuscript

Oncogene. Author manuscript; available in PMC 2009 October 09.

Published in final edited form as:

Oncogene. 2009 April 9; 28(14): 1694–1705. doi:10.1038/onc.2009.12.

VHL Type 2B gene mutation moderates HIF dosage *in vitro* and *in vivo*

C M Lee[1,2], **M Hickey**[3,4,5], **C A Sanford**[1], **C G McGuire**[1], **C L Cowey**[1], **M C Simon**[3,4,5], and **W K Rathmell**[1,2,*]

[1]Lineberger Comprehensive Cancer Center, University of North Carolina, Chapel Hill, NC 27599

[2]Curriculum in Genetics and Molecular Biology, University of North Carolina, Chapel Hill, NC 27599

[3]Abramson Family Cancer Research Institute, University of Pennsylvania School of Medicine, Philadelphia, PA 19104

[4]Cell and Molecular Biology Graduate Group, University of Pennsylvania School of Medicine, Philadelphia, PA 19104

[5]Howard Hughes Medical Institute, University of Pennsylvania School of Medicine, Philadelphia, PA 19104

Abstract

Von Hippel-Lindau (VHL) disease is caused by germline mutations in the *VHL* tumor suppressor gene, with Type 2B missense *VHL* mutations predisposing to renal cell carcinoma, hemangioblastoma, and pheochromocytoma. Type 2B mutant pVHL is predicted to be defective in hypoxia inducible factor (HIF)-α regulation. Murine embryonic stem (ES) cells in which the endogenous wild-type *Vhl* gene was replaced with the representative Type 2B *VHL* hotspot mutation R167Q ($Vhl^{2B/2B}$) displayed preserved physiologic regulation of both HIF factors with slightly more normoxic dysregulation of HIF-2α. Differentiated $Vhl^{2B/2B}$-derived teratomas over-expressed the joint HIF targets *Vegf* and *EglN3* but not the HIF-1α-specific target *Pfk1* and displayed a growth advantage over $Vhl^{-/-}$-derived teratomas, suggestive of a tight connection between perturbations in the degree and ratio of HIF-1α and HIF-2α stabilization and cell growth. $Vhl^{2B/2B}$ mice displayed mid-gestational embryonic lethality, while adult $Vhl^{2B/+}$ mice exhibited susceptibility to carcinogen-promoted renal neoplasia compared with wild-type littermates at twelve months. Our experiments support a model in which the representative Type 2B R167Q mutant pVhl produces a unique profile of HIF dysregulation, thereby promoting tissue-specific effects on cell growth, development, and tumor predisposition.

*Corresponding author: W. Kimryn Rathmell, Lineberger Comprehensive Cancer Center, The University of North Carolina at Chapel Hill, 450 West Drive, Room 21-237, Campus Box 7295, Chapel Hill, NC 27599-7295, Telephone: (919) 966-3522, Fax: (919) 966-8212, E-mail: rathmell@med.unc.edu.

Keywords

von Hippel-Lindau; hypoxia inducible factors; renal cell carcinoma

Introduction

Von Hippel-Lindau (VHL) disease is an autosomal dominant inherited cancer susceptibility syndrome resulting from germline mutation of the *VHL* tumor suppressor gene which affects 1 in 36,000 live births in the US (Maher et al., 1991; Neumann & Wiestler, 1991). Specific classes of *VHL* mutations predispose to different spectrums of morbidity- and mortality-causing clinical phenotypes of VHL disease: retinal and central nervous system (CNS) hemangioblastoma, pheochromocytoma/paraganglioma, and renal cell carcinoma with clear cell histology (ccRCC) (Crossey et al., 1994; Zbar et al., 1996). Type 1 *VHL* mutations predispose to ccRCC and hemangioblastoma (Gallou et al., 2004). Type 2 missense *VHL* mutations predispose to pheochromocytoma, either alone (Type 2C) or in combination with hemangioblastoma and a high (Type 2B) or low (Type 2A) risk of ccRCC (Clifford et al., 2001). Finally, individuals with homozygosity for the germline R200W *VHL* mutation develop Chuvash Polycythemia (CP), a rare benign congenital erythrocytosis with no associated cancer risk (Ang et al., 2002; Pastore et al., 2003).

The *VHL* gene encodes a 30 kDa protein, pVHL (Iliopoulos et al., 1995; Latif et al., 1993). Wild-type pVHL has been reported to play roles in diverse biological processes including acting as the recognition domain for an E3 ubiquitin ligase complex (Iwai et al., 1999; Lisztwan et al., 1999) composed of Elongins B and C (Duan et al., 1995; Kibel et al., 1995), cullin-2 (Pause *et al.*, 1997), ROC1 (Rbx1) (Kamura et al., 1999), and an E2 conjugating enzyme (Iwai et al., 1999; Kamura et al., 2000). pVHL E3 ligase activity targets hypoxia inducible factor (HIF)-α subunits (Cockman et al., 2000; Iliopoulos et al., 1996; Maxwell et al., 1999; Ohh et al., 2000), a family of transcription factor subunits including HIF-1α and HIF-2α.

HIF-1α and HIF-2α coordinate cellular and whole-organism responses to hypoxia and are controlled at the level of stability and activity by oxygen-dependent hydroxylation. In normoxic conditions, a family of prolyl hydroxylases (Bruick & McKnight, 2001; Epstein et al., 2001; Ivan et al., 2002; Ivan et al., 2001) mediates the hydroxylation of HIF-α prolyl residues (Huang et al., 2002; Huang et al., 1998; Jaakkola et al., 2001; Pugh et al., 1997), targeting HIF-α to pVHL for degradation (Hon et al., 2002; Min et al., 2002). In hypoxic conditions, the prolyl hydroxylases are inactive (Epstein et al., 2001; Jiang et al., 1997; Pugh et al., 1997), resulting in stabilized, transcriptionally active HIF-α. Stabilized HIF-α heterodimerizes with ARNT/HIF-1β (Jiang et al., 1996) to activate the transcription of target genes (Semenza et al., 1996; Tian et al., 1997). HIF-1α and HIF-2α target gene sets overlap in a highly context-dependent manner (Semenza, 2003), but HIF-1α uniquely activates glycolytic enzymes (Hu et al., 2003).

Several lines of evidence implicate the *VHL/HIF* axis in the initiation of renal tumorigenesis. First, biallelic inactivation of *VHL* and over-expression of HIF targets is observed in both VHL disease-associated renal lesions and also 70-90% of sporadic ccRCC

tumors (Banks et al., 2006; Foster et al., 1994; Kondo et al., 2002; Nickerson et al., 2008). Second, over-expression of HIF targets accounts for many histological and clinical features of ccRCC tumors, including their highly vascular natures and paraneoplastic erythrocytosis (Rathmell & Chen, 2008). Third, *Vhl* loss in primary cells directly results in upregulation of both HIF-1α and HIF-2α and recapitulates many features of RCC (Mack et al., 2003). Finally, emerging evidence points to the degree of HIF dysregulation impacting renal tumorigenesis. *In vitro* studies of cDNA expressed Type 2A and Type 2B mutant pVHL models revealed graded dysregulation of HIF-1α and HIF-2α (Clifford et al., 2001; Cockman et al., 2000), correlating with the degree of risk for ccRCC (Type 1≥ Type 2B > Type 2A) (Knauth et al., 2006; Li et al., 2007). Additionally, while Type 2B mutations are predicted to disrupt pVHL:Elongin C interactions, preservation of HIF ubiquitylation activity has been observed, which would provide a permissive environment for HIF regulation (Hacker et al, 2008). The profile of HIF dysregulation may also have ramifications for tumor predisposition, as selective HIF-2α stabilization has been observed in murine embryonic stem (ES) cells transgenic for a Type 2B mutant *VHL* gene (Rathmell et al., 2004). These systems in addition to demonstrating mutation specificity are sensitive to pVHL levels.

Existing mouse models of VHL disease utilize null (Gnarra et al., 1997) or conditional null (Haase et al., 2001; Ma et al., 2003) *Vhl* alleles, display homozygous embryonic lethality, and show a high penetrance of hepatic angiomas, uncommon in the human disease. A *Vhl* gene replacement model of Chuvash Polycythemia, however, was viable and conferred erythrocytosis in a milieu of very mild HIF-2α stabilization (Hickey et al., 2007). To examine the activities of mutant pVHL relevant to human cancer, particularly with respect to missense mutation-specific effects on HIF regulation, we undertook a gene replacement approach to study Type 2B VHL disease in a mouse model. This model provides the first opportunity to examine the effect of a VHL disease-causing missense mutations in its pre-malignant context and under endogenous transcriptional, translational, and post-translational regulation. Murine ES cells homozygous for a representative mutant 2B *Vhl* allele displayed mild HIF-2α stabilization but functionally preserved HIF-1α suppression. *In vivo*, while homozygosity for the mutant 2B *Vhl* allele conferred mid-gestational embryonic lethality, heterozygous $Vhl^{2B/+}$ mice were viable and susceptible to carcinogen-promoted renal adenocarcinoma. Our genetic knock-in mouse model thus provides a species-congruent cellular system and *in vivo* model in which to further examine the contributions of Type 2B *VHL* missense mutation to VHL disease-associated cancers.

Results

Generation and characterization of Type 2B *Vhl* ES cell lines

The Arginine 167 → Glutamine (R167Q) missense mutation is a hotspot in the human *VHL* gene with a tight genotype-phenotype correlation to Type 2B disease (Maher et al., 1991; Zbar et al., 1996). Localized to the pVHL α helical domain (Figure 1A), R167 is predicted to stabilize the α/β domain interface and interaction with Elongin C (Ohh et al., 1999; Stebbins et al., 1999). In the murine *Vhl* allele, this mutation corresponds to a guanine to alanine transition at position 518 (G518A).

To study the effect of 2B mutant pVhl on regulation of HIF-α and HIF targets, we targeted the endogenous murine *Vhl* locus with an R167Q mutant *Vhl* construct (Figure 1B) to generate $Vhl^{2B/+}$ and $Vhl^{2B/2B}$ ES cell lines. The targeting construct introduced a *HindIII* site, enabling verification of recombination by Southern analysis (Figure 1C), and the G518A mutation introduced a novel *HpyIV* restriction site for restriction-based PCR genotyping (Figure 1D). Quantitative RT-PCR analysis in $Vhl^{2B/2B}$ ES cells confirmed that 2B mutant *Vhl* was transcribed at wild-type levels (Figure 2A). $Vhl^{2B/+}$ cells expressed wild-type levels of pVhl, but $Vhl^{2B/2B}$ cells expressed greatly reduced levels of the 2B mutant pVhl (Figure 2B). A similar reduction in detectable 2B mutant pVhl was also observed by immunoblot with an antibody raised against an alternate epitope suggesting that reduced detection of 2B mutant pVhl was not due to epitope-masking alone. Rescue with MG-132 treatment was not observed, consistent with the reduced protein expression and incomplete MG-132 rescue observed in the Chuvash Polycythemia *Vhl* gene replacement model (Hickey et al., 2007).

Analysis of HIF and HIF target expression in Type 2B *Vhl* ES cells

The R167Q human pVHL mutation is predicted to destabilize the pVhl protein (Knauth et al., 2006) and to disrupt pVhl recruitment of Elongin C (Stebbins et al., 1999), resulting in HIF factor dysregulation. ES cells in the presence or absence of the chemical hypoxia mimetic cobalt chloride ($CoCl_2$) were examined for HIF-1α (Figure 2C) and HIF-2α (Figure 2D) protein levels by immunoblot. Wild-type and $Vhl^{2B/+}$ ES cells displayed low basal levels of HIF-1α and HIF-2α and responded to $CoCl_2$ exposure with induction of both factors. $Vhl^{-/-}$ ES cells displayed maximal stabilization of both HIF-1α and HIF-2α without further induction. In contrast, $Vhl^{2B/2B}$ ES cells retained physiologic induction of both HIF-α factors with $CoCl_2$. While normoxic HIF-1α levels in $Vhl^{2B/2B}$ cells were similar to wild-type cells in independently-derived clones (Figure 2C), normoxic HIF-2α levels tended to be modestly elevated (Figure 2D). Qualitative comparisons were confirmed by densitometry analysis (Supplemental Figure 1).

HIF-2α is transcriptionally inactive in ES cells (Hu et al., 2006). To determine whether $Vhl^{2B/2B}$ ES cells activate transcription of HIF target genes, we performed quantitative (q) RT-PCR for four known HIF target mRNAs (Figure 2E): the joint HIF-1α and HIF-2α targets *vascular endothelial growth factor* (*Vegf*), *glucose transporter 1* (*Glut1*), and *prolyl hydroxylase three* (*EglN3)* and the HIF-1α-specific glycolytic enzyme *phosphofructokinase (Pfk1*). $Vhl^{-/-}$ ES cells displayed transcription of all four HIF target mRNAs relative to wild-type J1 cells ($p<0.05$): *Vegf* (4.26-fold), *Glut1* (2.66-fold), *EglN3* (11.80-fold), and *Pfk1* (2.32-fold). Two independently-derived $Vhl^{2B/2B}$ clones, in contrast, failed to significantly over-transcribe any of the four HIF targets, consistent with the observation that $Vhl^{2B/2B}$ ES cells exhibit wild-type HIF-1α expression. Mirroring the qRT-PCR results, $Vhl^{-/-}$ ES cells secreted robust levels of Vegf protein (4.4-fold) compared to wild-type ($p<0.01$), while $Vhl^{2B/2B}$ ES cells did not secrete measurable Vegf (Figure 2F).

Type 2B *Vhl* promotes teratoma growth and vascularization

To observe the functional effects of Type 2B *Vhl* mutation, we differentiated our panel of ES cells in a teratoma assay. As expected from previous studies (Rathmell et al., 2004),

Vhl$^{-/-}$-derived teratomas displayed a growth disadvantage. In contrast, the presence of one or two Type 2B *Vhl* alleles conferred a persistent growth advantage, such that *Vhl*$^{2B/2B}$-derived teratomas grew faster than *Vhl*$^{2B/+}$-derived teratomas, which in turn grew faster than wild-type teratomas (Figure 3A). At harvest, J1, *Vhl*$^{-/-}$, and *Vhl*$^{2B/+}$ teratomas were well-encapsulated, while *Vhl*$^{2B/2B}$ teratomas adhered to the overlying skin (not shown). *Vhl*$^{2B/2B}$ teratomas (Figure 3B, left) were also grossly hemorrhagic compared to *Vhl*$^{2B/+}$ (Figure 3B, right) teratomas. Histologically, *Vhl*$^{-/-}$ teratomas were characterized by hemangioma (*) formation (Figure 3E), which was markedly enhanced in *Vhl*$^{2B/2B}$ teratomas (Figure 3F).

To determine whether Type 2B mutant pVhl preserves HIF regulation *in vivo*, teratomas were analyzed for HIF-1α and HIF-2α protein expression by immunoblot, confirming low levels of both HIF factors (Supplemental Figure 2). To evaluate the effect on target gene expression, we performed quantitative RT-PCR for the panel of HIF target genes described above in three independent sets of teratomas. In one representative set (Figure 3G), the *Vhl*$^{-/-}$ teratoma displayed highly significant ($p<0.001$) over-expression of three of the four HIF targets relative to the J1 teratoma: *Vegf* (1.99-fold), *EglN3* (3.15-fold), and *Pfk1* (2.12-fold). In contrast to ES cells, the *Vhl*$^{2B/2B}$-derived teratoma exhibited significant over-expression of both *EglN3* (1.46-fold, $p<0.05$) and *Vegf* (1.87-fold, $p<0.001$) but failed to over-express the HIF-1α-specific target *Pfk1*. *Glut1* expression was not elevated for either *Vhl* mutant in this differentiated system.

To explore the differences in vascular proclivities between *Vhl*$^{-/-}$ and *Vhl*$^{2B/2B}$ teratomas, we performed a screen for candidate angiogenesis-related genes (Supplemental Table 1 and Figure 4). Four novel angiogenesis-related candidate genes, in addition to *Vegfa*, were uncovered in the candidate screen and validated by qRT-PCR with independent primers : *vascular endothelial (VE)-cadherin* (*Cdh5*), the TgfβR endothelial co-receptor *endoglin* (*Eng*), *Vegf receptor 2* (*Kdr*), and the Vegfr2 co-receptor *neuropilin-1* (*Nrp1*). All four are considered direct HIF targets (Brusselmans et al., 2005; Elvert et al., 2003; Le Bras et al., 2007; Sanchez-Elsner et al., 2002). While both the *Vhl*$^{-/-}$ and *Vhl*$^{2B/2B}$ teratomas significantly over-expressed *Cdh5*, *Eng*, and *Kdr* relative to the J1 teratoma, the *Vhl*$^{2B/2B}$ teratoma additionally significantly ($p<0.001$) over-expressed *Nrp1* relative to both J1 and *Vhl*$^{-/-}$ (Figure 4).

Homozygosity for Type 2B *Vhl* confers embryonic lethality

To examine 2B mutant pVhl function in murine development *in vivo*, we derived *Vhl*$^{2B/+}$ knock-in mice from our targeted murine ES cells. Inter-heterozygous matings resulted in a 2:1 ratio of *Vhl*$^{2B/+}$ to wild-type pups and a complete absence of *Vhl*$^{2B/2B}$ pups (Table 1). To pinpoint the window of *Vhl*$^{2B/2B}$ intrauterine demise, we genotyped embryos resulting from timed matings at embryonic day (E) 9.5 and E10.5. While *Vhl*$^{2B/2B}$ embryos were present at near-expected levels at E9.5, only one *Vhl*$^{2B/2B}$ embryo (3%) survived at E10.5. Because reliance switches from yolk sac to placenta around E9.5 (Alvarez-Silva et al., 2003), *Vhl*$^{2B/2B}$ embryonic lethality observed at E9.5-E10.5 implicates placental failure.

Vhl$^{-/-}$ embryos display embryonic lethality at E9.5-E12.5 due to an embryonic-origin defect in placental labyrinth vascularization. While the presumptive *Vhl*$^{-/-}$ labyrinth is normal in

histological appearance at E9.5, *Vhl*$^{-/-}$ allantoic vessels fail to invade the chorionic plate, preventing induction of chorionic plate trophoblast cell differentiation into syncitiotrophoblast cells and later manifesting as an absence of fetal blood spaces in the labyrinth at E10.5 (Gnarra et al., 1997). To visualize whether the 2B mutant *Vhl* allele acts similarly to the null allele in the placenta, we compared wild-type (not shown), *Vhl*$^{2B/+}$, and *Vhl*$^{2B/2B}$ placentas by H&E for morphology and IHC for pVhl and the HIF target Vegfa. By H&E, representative E9.5 *Vhl*$^{2B/+}$ (Figure 5A) and *Vhl*$^{2B/2B}$ (Figure 5D) placentas displayed comparable chorionic villous fold formation and maternal red blood cell content in the spongiotrophoblast layer, but allantoic vessels, demarcated by the presence of nucleated fetal red blood cells (*), invaded the chorionic villi to a lesser extent in the *Vhl*$^{2B/2B}$ placenta. Despite the reduced Type 2B pVhl levels observed by immunoblot in *Vhl*$^{2B/2B}$ ES cells, spongiotrophoblast and giant cell pVhl expression was comparable between representative *Vhl*$^{2B/2B}$ (Figure 5E) and *Vhl*$^{2B/+}$ (Figure 5B) placentas by IHC. Finally, consistent with findings in *Vhl*$^{-/-}$ placentas at E10.5 (Gnarra et al., 1997), *Vhl*$^{2B/2B}$ placenta (Figure 5F) displayed absent or greatly reduced spongiotrophoblast and giant cell Vegf expression relative to *Vhl*$^{2B/+}$ (Figure 5C) by IHC. While perhaps counter-intuitive, evidence supports decreased Vegf expression as a marker of placental failure rather than an indicator of HIF dysregulation in the murine placenta (Voss et al., 2000).

Because E9.5 embryos were the only *Vhl*$^{2B/2B}$ animal tissues available for molecular study, we used these tissues to analyze the competence of Type 2B pVhl to regulate HIF target genes *in vivo*. Though *Vhl*$^{2B/2B}$ embryos are grossly and histologically normal at E9.5, we hypothesized that they might still demonstrate subtle HIF target gene dysregulation. Quantitative RT-PCR on three *Vhl*$^{2B/2B}$ E9.5 embryos showed significant ($p<0.05$) over-expression of the four HIF target genes studied relative to a *Vhl*$^{2B/+}$ E9.5 embryo, paralleling the effect of *Vhl* mutation on HIF-regulated signaling observed in the differentiated teratoma model system (Figure 5G): *Vegf* (average 1.54-fold), *Glut1* (average 2.60-fold), *EglN3* (average 3.53-fold), and *Pfk1* (average 1.88-fold). In notable contrast to ES cells and teratomas and in keeping with the reported highly tissue- and context-specific transcriptional effects of HIF stabilization, homozygosity for the 2B *Vhl* allele produced sufficient HIF-1α dysregulation to permit over-expression of the HIF-1α-specific target *Pfk1* in the E9.5 embryo, with potential contribution by physiologic embryonic hypoxia.

Heterozygous Type 2B *Vhl* mice develop renal cysts

As Type 2B VHL disease predisposes to pheochromocytoma, hemangioblastoma, and ccRCC in humans, *Vhl*$^{2B/+}$ mice (n=105) were aged to three, six, nine, twelve, and eighteen months and observed for tumor susceptibility. Representative H&E images of *Vhl*$^{2B/+}$ tissues at twelve months are presented in Figure 6 (A-C). Similar to prior models, *Vhl*$^{2B/+}$ mice displayed frequent enlarged vessels (angiectasis) in the kidney and adrenal gland (Figure 6B, *) (Gnarra et al., 1997; Haase et al., 2001; Ma et al., 2003) and renal cortical microcysts (3%, Figure 6A, Cy) (Haase et al., 2001). Renal cortical cysts were not observed in wild-type littermates. In contrast to prior studies, *Vhl*$^{2B/+}$ liver histology was uniformly normal (Figure 6C).

Transplacental mutagenesis promotes renal tumorigenesis in Type 2B *Vhl* mice

We hypothesized that accelerating somatic mutations via mutagenesis might reveal predisposition to cancer development in $Vhl^{2B/+}$ mice. Transplacental N-ethyl-N-nitrosourea (ENU) mutagenesis has been used successfully to augment renal cystogenesis in mouse models of Tuberous Sclerosis (Kobayashi et al., 1999), another renal tumor predisposition syndrome, and therefore was an ideal method for accelerating progression in our model. Wild-type and $Vhl^{2B/+}$ embryos from timed inter-heterozygous matings were treated with ENU at E14.5 and allowed to age to four (n=12) and twelve months (n=24) in a pilot study. At sacrifice, grossly abnormal organs and organs of interest were harvested. Renal lesions observed in mutagenized mice are summarized in Table 2.

At four months, both wild-type (2/4) and $Vhl^{2B/+}$ (6/8) mutagenized mice displayed macroscopic subpleural lung nodules, indicating successful ENU mutagenesis (Miller, 2004). Both wild-type and $Vhl^{2B/+}$ mutagenized mice displayed simple and papillary cortical renal microcysts on H&E-stained sections, suggesting that ENU mutagenesis effectively promotes benign renal cyst formation in this C57BL/6 genetic background. While all three papillary renal cysts observed in mutagenized wild-type mice displayed benign histology, the papillary cyst in observed in a mutagenized $Vhl^{2B/+}$ mouse displayed pre-neoplastic changes (not shown).

At twelve months, histological findings in wild-type mutagenized mice were limited to benign papillary cysts (Figure 6D). However, $Vhl^{2B/+}$ mutagenized mice (2/10) developed pathological findings typical of VHL disease. One $Vhl^{2B/+}$ mouse developed a borderline clear-cell adenoma/adenocarcinoma (Figure 6E) featuring a large nest of cells (alveolus) with clear-cell histology, vascular stroma, and absent tubular architecture as well as several clear-cell alveoli invading into the underlying renal cortex. A second affected $Vhl^{2B/+}$ mouse developed adenocarcinoma (Figure 6F) featuring nests of clear cells, central necrosis, absent tubular architecture, vascular stroma, and a poorly defined border. Statistical analysis suggested that *Vhl* mutation correlated with or trended toward development of neoplasia at 12 months (Pearson's χ^2 p=0.037, Fisher's exact test p=0.101).

Discussion

Germline Type 2B missense mutations in *VHL* predispose to ccRCC, CNS and retinal hemangioblastoma, and pheochromocytoma and paraganglioma. In our murine gene replacement system, which models one VHL type 2B disease mutation, R167Q, generated a unique pattern of HIF-1α and HIF-2α dysregulation, differing from *Vhl*-null both in degree and ratio of HIF stabilization as well as in functional outcome in *in vitro* and *in vivo* studies.

Our gene replacement system takes advantage of the euploid genetic background of murine ES cells and avoids the potential mouse-human interactions and over- and mis-expression artifacts inherent to transgenic models. We observed reduced levels of 2B mutant pVhl protein in homozygous ES cells, supporting the hypothesis that ccRCC-predisposing *VHL* missense mutations produce less stable proteins, as posited on the basis of structure analysis (Knauth et al., 2006; Stebbins et al., 1999). In contrast to $Vhl^{-/-}$ ES cells, $Vhl^{2B/2B}$ knock-in ES cells expressed low basal levels of HIF-1α and HIF-2α and induced both subunits

physiologically in response to the hypoxia mimetic $CoCl_2$. Consistent with this finding, *Vhl*$^{2B/2B}$ ES cells displayed wild-type levels of four HIF target genes studied, suggesting that HIF-1α levels in *Vhl*$^{2B/2B}$ cells failed to surpass a threshold required for transcriptional activation at target promoters in this cell type.

The differentiated teratoma system allowed observation of 2B mutant pVhl function in a setting permissive for both HIF-1α and HIF-2α transcriptional activity. Previous work in *Vhl*$^{-/-}$ teratomas has demonstrated that maximal activation of both HIF-1α and HIF-2α promotes angiogenesis but retards three-dimensional tumor growth (Mack et al., 2003). Genetic knock-out of HIF-1α (Carmeliet et al., 1998) or replacement of HIF-1α with HIF-2α (Covello et al., 2005) in teratomas enhances tumor growth and implicates HIF-1α as the growth-suppressive factor in this assay. In our studies, *Vhl*$^{-/-}$ teratomas likewise displayed a growth disadvantage relative to wild-type and additionally featured over-expression of the joint HIF targets *Vegfa* and *EglN3* and the HIF-1α-specific target *Pfk1*, all indicating HIF-1α and HIF-2α stabilization. *Vhl*$^{2B/2B}$ teratomas, in contrast, displayed a marked growth advantage relative to wild-type, and over-expression of *Vegfa* and *EglN3*, but not *Pfk1*, suggestive of sub-threshold HIF-1α but sufficient HIF-2α stabilization to promote transcriptional activity.

The placental failure and lethality observed in *Vhl*$^{2B/2B}$ embryos at E9.5-E10.5 was consistent with severely hypomorphic mutant pVhl function in the embryonic allantoic endothelium. Reduced pVhl stability alone is unlikely to be the cause of *Vhl*$^{2B/2B}$ embryonic lethality. First, 2B mutant pVhl levels in the E9.5 *Vhl*$^{2B/2B}$ placenta were similar to pVhl levels observed in the E9.5 *Vhl*$^{2B/+}$ placenta by IHC. Second, *Vhl*$^{CP/CP}$ mice are viable despite the measurable instability of R200W (CP) pVhl both *in vitro* and in murine tissues (Hickey et al., 2007). Finally, there is evidence of more severe HIF dysregulation in this *in vivo* system, with evidence of induction of the HIF-1α-specific target *Pfk1*, indicating both HIF-1α and HIF-2α stabilization. Thus, while it remains possible that the degree of pVhl reduction has a threshold effect on early developmental events, the reduced levels in these models serves to unmask added levels of regulation of the HIF transcriptional network.

Vhl$^{2B/+}$ mice developed renal cysts with frequency similar to that observed in *Vhl*$^{+/-}$ mice (∼3%) and likewise failed to develop dysplasia or renal adenocarcinoma, indicating that *Vhl* mutation alone is insufficient for invasive renal tumor formation in the murine kidney To accelerate the accumulation of somatic mutations in this mouse model and reveal tumor predisposition, we mutagenized *Vhl*-initiated and wild-type littermate mice with transplacental ENU. At twelve months post-ENU, renal adenocarcinoma was observed in mutagenized *Vhl*$^{2B/+}$ mice, representing the first demonstration of this tumor in a genetically-predisposed mouse model and validating *Vhl* mutation as a tumor-initiating event in the development of RCC.

Our gene replacement model of the representative Type 2B R167Q *Vhl* mutation bolsters emerging evidence that relative HIF-1α and HIF-2α protein abundance modulates the VHL Disease clinical phenotype and provides motivation for identifying the relevant genetic events involved in progressing *Vhl*-initiated tumors to invasive disease. More broadly, our *Vhl* gene replacement model provides a comprehensive species-congruent system for future

investigations of mutant pVhl HIF and non-HIF functions underpinning human VHL Disease both *in vitro* and *in vivo*.

Materials and Methods

Generation of Vhl Type 2B ES cell lines and heterozygous mice

Vhl exons 2 and 3 (E2 and E3) were cloned into targeting and mutagenesis vectors, respectively, from a BAC clone as previously described (Covello et al., 2005; Hickey et al., 2007). PCR-based site-directed mutagenesis of G→A at position 518 was performed using forward primer 5′-AGAGCCTGGTCAAGCCTGAGAACTA-3′ and reverse primer 5′-GCACAACCTGAAGGCACCGCTCTTT-3′. The G518A mutant E3 fragment was then cloned into pLNT-E2 adjacent to the neo^R cassette (pLNT-E2-E3) and reconfirmed with bidirectional sequencing.

The pLNT-E2-E3 targeting construct (Figure 1B) was electroporated into *Vhl* wild-type J1 strain Sv/129 ES cells for gene replacement at the endogenous murine *Vhl* locus. Homologous recombinants heterozygous for the $Vhl^{2B\ neo\text{-}in}$ allele were selected by gancyclovir and neomycin resistance, and positive clones confirmed by Southern blot analysis. Conversion of the second *Vhl* allele was achieved by selection with increasing amounts of neomycin to yield ES cells homozygous for the $Vhl^{2B\ neo\text{-}in}$ allele. $Vhl^{2B\ neo\text{-}in/+}$ and $Vhl^{2B\ neo\text{-}in/2B\ neo\text{-}in}$ ES cells were transiently transfected with a cre-expressing vector to remove the floxed neo^R cassette. The ES cells were screened at each stage by Southern blot for *in vitro* and *in vivo* studies of Type 2B mutant pVhl function.

Animal Models Core (University of Pennsylvania) staff injected karyotyped $Vhl^{2B\ neo\text{-}in/+}$ ES cells into C57BL/6 blastocysts. The chimeric blastocysts were then implanted in pseudopregnant C57BL/6 females. Highly chimeric mice (F0) were selected by Agouti coat color for crossing to C57BL/6 females. Germline transmission of the targeted allele to Agouti offspring (F1) was confirmed by Southern blot. A $Vhl^{2B\ neo\text{-}in/+}$ line was crossed to a cre deleter mouse strain (EIIa-cre) (Williams-Simons & Westphal, 1999) for multiple generations, with excision of the floxed neo^R cassette verified by Southern blot, and then backcrossed to C57BL/6 to make a $Vhl^{2B/+}$ founder line. All subsequent generations were genotyped by restriction PCR utilizing PCR primers flanking a novel HpyIV restriction site introduced by the G518A *Vhl* mutation (Figure 1D).

All mouse procedures were approved by the University of Pennsylvania and University of North Carolina Institutional Animal Care and Use Committees.

Cell Culture Studies

Cell culture studies were performed at 37°C, 5% CO_2. ES cell lines were maintained in ES media consisting of high glucose Dulbecco's Modified Eagle Medium (Gibco, Carlsbad, CA, USA) supplemented with 5% fetal bovine serum, L-glutamine, β-mercaptoethanol, non-essential amino acids, and leukemia inhibitory factor (LIF), and grown on gelatin-coated tissue culture-grade plates (Corning, Corning, NY, USA). For chemical hypoxia mimetic experiments, cells were grown in the presence or absence of $CoCl_2$ (100 μM) for four hours.

For proteasome inhibition experiments, cells were treated with vehicle (DMSO) or MG-132 (5 μM, Calbiochem, San Diego, CA, USA) for four hours.

For *in vivo* teratoma studies, undifferentiated ES cells of each genotype (5×10^6) were injected subcutaneously into the flanks of *nu/nu* mice (Taconic Labs, Hudson, NY, USA) and allowed to grow for six weeks with weekly caliper measurements of tumor size. Harvested tumors were bisected and either flash-frozen in liquid nitrogen for molecular analysis or formalin-fixed and paraffin-embedded for histological analysis.

Molecular analysis of Vhl, HIF, and HIF targets

Whole-cell protein extracts for immunoblot were prepared in NET lysis buffer (20mM Tris, 100mM NaCl, 1mM EDTA, 1% NP-40) and quantitated by Bradford assay. Immunoblot primary antibodies used were: pVhl (M20 and FL181, Santa Cruz Biotechnology, Santa Cruz, CA, USA), HIF-1α (10006421, Cayman Chemical, Ann Arbor, MI, USA), HIF-2α (NB100-122, Novus Biologicals, Littleton, CO, USA), and eEF2 (Cell Signaling Technology, Danvers, MA, USA). Murine Vegf ELISA was performed on conditioned medium from cultured ES cells (R & D Systems, Minneapolis, MN, USA).

RNA isolation from ES cells, teratomas, and E9.5 embryos was performed using the RNeasy Mini system according to manufacturer's instructions (Qiagen, Germantown, MD, USA) and quantified by UV spectroscopy. cDNA was prepared from 0.5μg of RNA using Superscript reverse transcription reagents (Stratagene, Cedar Creek, TX, USA). Quantitative RT-PCR was performed in triplicate using stock commercial primer-probe sets for *Vhl*, *Vegfa*, *Glut1*, *EglN3*, *Pfk1*, and *18S* ribosomal subunit according to manufacturer's instructions (Applied Biosystems, Foster City, CA, USA). A candidate screen for teratoma hemangioma-associated genes was performed in triplicate on the RT^2 Profiler Mouse Angiogenesis Array using cycle parameters according to manufacturer's instructions (SABiosciences, Frederick, MD, USA). Genes identified for further validation were analyzed by quantitative RT-PCR in triplicate using stock commercial primer-probe sets for *Cdh5*, *Eng*, *Kdr*, *Nrp1*, *Vegfc*, and *18S* ribosomal subunit and cycle parameters according to manufacturer's instructions (Applied Biosystems). All quantitative RT-PCR output raw cycle thresholds were normalized to the internal *18S* ribosomal RNA standard.

Embryonic lethality and transplacental ethyl nitrosourea (ENU) mutagenesis studies

$Vhl^{2B/+}$ mice were set up for timed inter-heterozygous mating. Embryonic day (E) 0.5 was defined as noon on the day the vaginal plug was observed, and embryos and placentas were harvested at E9.5 and E10.5. For placental studies, embryos were examined for gross defects and genotyped by restriction PCR, and placentas were processed for histological examination. For embryonic studies, E9.5 embryos were used for both RNA extraction and genotyping by restriction PCR.

For transplacental mutagenesis studies, intraperitoneal (i.p.) injection of 50 mg/kg ENU (Sigma, St. Louis, MO, USA) dissolved in ethanol was administered to the pregnant dam at E14.5 (Kobayashi et al., 1999). Mutagenized $Vhl^{2B/+}$ and wild-type littermates were aged in four- and twelve-month cohorts and sacrificed for gross and histological examination.

Histological analysis of murine tissues

Harvested tissues were fixed in 10% buffered formalin. Paraffin-embedded tissues were sectioned and stained with hematoxylin and eosin (H&E) or for pVhl (FL181) or Vegfa (VG-1, Santa Cruz).

Statistical analysis

A two-tailed Student's *t* test was used to make paired comparisons for quantitative RT-PCR and Vegf ELISA data. A value of $p \leq 0.05$ was used as the threshold for statistical significance. Pearson's χ^2 test and Fisher's exact test were used to compare development of neoplasia in wild-type versus *Vhl*-mutant mutagenized mice.

Supplementary Material

Refer to Web version on PubMed Central for supplementary material.

Acknowledgements

We thank Dr. T. Van Dyke and members of her laboratory, Dr. I. Davis, and Dr. W. Y. Kim for many helpful discussions. This work was supported by the V Foundation, the American Cancer Society, the VHL Family Alliance, and the NCI K08098410 and R01121781 (WKR); by the Howard Hughes Medical Institute (MCS, MMH); and by the NIEHS F30015248 (CML).

References

Alvarez-Silva M, Belo-Diabangouaya P, Salaun J, Dieterlen-Lievre F. Development. 2003; 130:5437–44. [PubMed: 14507780]

Ang SO, Chen H, Hirota K, Gordeuk VR, Jelinek J, Guan Y, Liu E, Sergueeva AI, Miasnikova GY, Mole D, Maxwell PH, Stockton DW, Semenza GL, Prchal JT. Nat Genet. 2002; 32:614–21. [PubMed: 12415268]

Banks RE, Tirukonda P, Taylor C, Hornigold N, Astuti D, Cohen D, Maher ER, Stanley AJ, Harnden P, Joyce A, Knowles M, Selby PJ. Cancer Res. 2006; 66:2000–11. [PubMed: 16488999]

Bruick RK, McKnight SL. Science. 2001; 294:1337–40. [PubMed: 11598268]

Brusselmans K, Bono F, Collen D, Herbert JM, Carmeliet P, Dewerchin M. J Biol Chem. 2005; 280:3493–9. [PubMed: 15572379]

Carmeliet P, Dor Y, Herbert JM, Fukumura D, Brusselmans K, Dewerchin M, Neeman M, Bono F, Abramovitch R, Maxwell P, Koch CJ, Ratcliffe P, Moons L, Jain RK, Collen D, Keshert E. Nature. 1998; 394:485–90. [PubMed: 9697772]

Clifford SC, Cockman ME, Smallwood AC, Mole DR, Woodward ER, Maxwell PH, Ratcliffe PJ, Maher ER. Hum Mol Genet. 2001; 10:1029–38. [PubMed: 11331613]

Cockman ME, Masson N, Mole DR, Jaakkola P, Chang GW, Clifford SC, Maher ER, Pugh CW, Ratcliffe PJ, Maxwell PH. J Biol Chem. 2000; 275:25733–41. [PubMed: 10823831]

Covello KL, Simon MC, Keith B. Cancer Res. 2005; 65:2277–86. [PubMed: 15781641]

Crossey PA, Richards FM, Foster K, Green JS, Prowse A, Latif F, Lerman MI, Zbar B, Affara NA, Ferguson-Smith MA, et al. Hum Mol Genet. 1994; 3:1303–8. [PubMed: 7987306]

Duan DR, Pause A, Burgess WH, Aso T, Chen DY, Garrett KP, Conaway RC, Conaway JW, Linehan WM, Klausner RD. Science. 1995; 269:1402–6. [PubMed: 7660122]

Elvert G, Kappel A, Heidenreich R, Englmeier U, Lanz S, Acker T, Rauter M, Plate K, Sieweke M, Breier G, Flamme I. J Biol Chem. 2003; 278:7520–30. [PubMed: 12464608]

Epstein AC, Gleadle JM, McNeill LA, Hewitson KS, O'Rourke J, Mole DR, Mukherji M, Metzen E, Wilson MI, Dhanda A, Tian YM, Masson N, Hamilton DL, Jaakkola P, Barstead R, Hodgkin J, Maxwell PH, Pugh CW, Schofield CJ, Ratcliffe PJ. Cell. 2001; 107:43–54. [PubMed: 11595184]

Foster K, Prowse A, van den Berg A, Fleming S, Hulsbeek MM, Crossey PA, Richards FM, Cairns P, Affara NA, Ferguson-Smith MA, et al. Hum Mol Genet. 1994; 3:2169–73. [PubMed: 7881415]

Gallou C, Chauveau D, Richard S, Joly D, Giraud S, Olschwang S, Martin N, Saquet C, Chretien Y, Mejean A, Correas JM, Benoit G, Colombeau P, Grunfeld JP, Junien C, Beroud C. Hum Mutat. 2004; 24:215–24. [PubMed: 15300849]

Gnarra JR, Ward JM, Porter FD, Wagner JR, Devor DE, Grinberg A, Emmert-Buck MR, Westphal H, Klausner RD, Linehan WM. Proc Natl Acad Sci U S A. 1997; 94:9102–7. [PubMed: 9256442]

Haase VH, Glickman JN, Socolovsky M, Jaenisch R. Proc Natl Acad Sci U S A. 2001; 98:1583–8. [PubMed: 11171994]

Hacker KE, Lee CM, Rathmell WK. PLoS One. 2008; 3:e3801. [PubMed: 19030229]

Hickey MM, Lam JC, Bezman NA, Rathmell WK, Simon MC. J Clin Invest. 2007; 117:3879–89. [PubMed: 17992257]

Hon WC, Wilson MI, Harlos K, Claridge TD, Schofield CJ, Pugh CW, Maxwell PH, Ratcliffe PJ, Stuart DI, Jones EY. Nature. 2002; 417:975–8. [PubMed: 12050673]

Hu CJ, Iyer S, Sataur A, Covello KL, Chodosh LA, Simon MC. Mol Cell Biol. 2006; 26:3514–26. [PubMed: 16611993]

Hu CJ, Wang LY, Chodosh LA, Keith B, Simon MC. Mol Cell Biol. 2003; 23:9361–74. [PubMed: 14645546]

Huang J, Zhao Q, Mooney SM, Lee FS. J Biol Chem. 2002; 277:39792–800. [PubMed: 12181324]

Huang LE, Gu J, Schau M, Bunn HF. Proc Natl Acad Sci U S A. 1998; 95:7987–92. [PubMed: 9653127]

Iliopoulos O, Kibel A, Gray S, Kaelin WG Jr. Nat Med. 1995; 1:822–6. [PubMed: 7585187]

Iliopoulos O, Levy AP, Jiang C, Kaelin WG Jr. Goldberg MA. Proc Natl Acad Sci U S A. 1996; 93:10595–9. [PubMed: 8855223]

Ivan M, Haberberger T, Gervasi DC, Michelson KS, Gunzler V, Kondo K, Yang H, Sorokina I, Conaway RC, Conaway JW, Kaelin WG Jr. Proc Natl Acad Sci U S A. 2002; 99:13459–64. [PubMed: 12351678]

Ivan M, Kondo K, Yang H, Kim W, Valiando J, Ohh M, Salic A, Asara JM, Lane WS, Kaelin WG Jr. Science. 2001; 292:464–8. [PubMed: 11292862]

Iwai K, Yamanaka K, Kamura T, Minato N, Conaway RC, Conaway JW, Klausner RD, Pause A. Proc Natl Acad Sci U S A. 1999; 96:12436–41. [PubMed: 10535940]

Jaakkola P, Mole DR, Tian YM, Wilson MI, Gielbert J, Gaskell SJ, Kriegsheim A, Hebestreit HF, Mukherji M, Schofield CJ, Maxwell PH, Pugh CW, Ratcliffe PJ. Science. 2001; 292:468–72. [PubMed: 11292861]

Jiang BH, Rue E, Wang GL, Roe R, Semenza GL. J Biol Chem. 1996; 271:17771–8. [PubMed: 8663540]

Jiang BH, Zheng JZ, Leung SW, Roe R, Semenza GL. J Biol Chem. 1997; 272:19253–60. [PubMed: 9235919]

Kamura T, Koepp DM, Conrad MN, Skowyra D, Moreland RJ, Iliopoulos O, Lane WS, Kaelin WG Jr. Elledge SJ, Conaway RC, Harper JW, Conaway JW. Science. 1999; 284:657–61. [PubMed: 10213691]

Kamura T, Sato S, Iwai K, Czyzyk-Krzeska M, Conaway RC, Conaway JW. Proc Natl Acad Sci U S A. 2000; 97:10430–5. [PubMed: 10973499]

Kibel A, Iliopoulos O, DeCaprio JA, Kaelin WG Jr. Science. 1995; 269:1444–6. [PubMed: 7660130]

Knauth K, Bex C, Jemth P, Buchberger A. Oncogene. 2006; 25:370–7. [PubMed: 16261165]

Kobayashi T, Minowa O, Kuno J, Mitani H, Hino O, Noda T. Cancer Res. 1999; 59:1206–11. [PubMed: 10096549]

Kondo K, Yao M, Yoshida M, Kishida T, Shuin T, Miura T, Moriyama M, Kobayashi K, Sakai N, Kaneko S, Kawakami S, Baba M, Nakaigawa N, Nagashima Y, Nakatani Y, Hosaka M. Genes Chromosomes Cancer. 2002; 34:58–68. [PubMed: 11921283]

Latif F, Tory K, Gnarra J, Yao M, Duh FM, Orcutt ML, Stackhouse T, Kuzmin I, Modi W, Geil L, et al. Science. 1993; 260:1317–20. [PubMed: 8493574]

Le Bras A, Lionneton F, Mattot V, Lelievre E, Caetano B, Spruyt N, Soncin F. Oncogene. 2007; 26:7480–9. [PubMed: 17563748]

Li L, Zhang L, Zhang X, Yan Q, Minamishima YA, Olumi AF, Mao M, Bartz S, Kaelin WG Jr. Mol Cell Biol. 2007; 27:5381–92. [PubMed: 17526729]

Lisztwan J, Imbert G, Wirbelauer C, Gstaiger M, Krek W. Genes Dev. 1999; 13:1822–33. [PubMed: 10421634]

Ma W, Tessarollo L, Hong SB, Baba M, Southon E, Back TC, Spence S, Lobe CG, Sharma N, Maher GW, Pack S, Vortmeyer AO, Guo C, Zbar B, Schmidt LS. Cancer Res. 2003; 63:5320–8. [PubMed: 14500363]

Mack FA, Rathmell WK, Arsham AM, Gnarra J, Keith B, Simon MC. Cancer Cell. 2003; 3:75–88. [PubMed: 12559177]

Maher ER, Iselius L, Yates JR, Littler M, Benjamin C, Harris R, Sampson J, Williams A, Ferguson-Smith MA, Morton N. J Med Genet. 1991; 28:443–7. [PubMed: 1895313]

Maxwell PH, Wiesener MS, Chang GW, Clifford SC, Vaux EC, Cockman ME, Wykoff CC, Pugh CW, Maher ER, Ratcliffe PJ. Nature. 1999; 399:271–5. [PubMed: 10353251]

Miller MS. Toxicol Appl Pharmacol. 2004; 198:95–110. [PubMed: 15236948]

Min JH, Yang H, Ivan M, Gertler F, Kaelin WG Jr. Pavletich NP. Science. 2002; 296:1886–9. [PubMed: 12004076]

Neumann HP, Wiestler OD. Lancet. 1991; 337:1052–4. [PubMed: 1673491]

Nickerson ML, Jaeger E, Shi Y, Durocher JA, Mahurkar S, Zaridze D, Matveev V, Janout V, Kollarova H, Bencko V, Navratilova M, Szeszenia-Dabrowska N, Mates D, Mukeria A, Holcatova I, Schmidt LS, Toro JR, Karami S, Hung R, Gerard GF, Linehan WM, Merino M, Zbar B, Boffetta P, Brennan P, Rothman N, Chow WH, Waldman FM, Moore LE. Clin Cancer Res. 2008; 14:4726–34. [PubMed: 18676741]

Ohh M, Park CW, Ivan M, Hoffman MA, Kim TY, Huang LE, Pavletich N, Chau V, Kaelin WG. Nat Cell Biol. 2000; 2:423–7. [PubMed: 10878807]

Ohh M, Takagi Y, Aso T, Stebbins CE, Pavletich NP, Zbar B, Conaway RC, Conaway JW, Kaelin WG Jr. J Clin Invest. 1999; 104:1583–91. [PubMed: 10587522]

Pastore YD, Jelinek J, Ang S, Guan Y, Liu E, Jedlickova K, Krishnamurti L, Prchal JT. Blood. 2003; 101:1591–5. [PubMed: 12393546]

Pause A, Lee S, Worrell RA, Chen DY, Burgess WH, Linehan WM, Klausner RD. Proc Natl Acad Sci U S A. 1997; 94:2156–61. [PubMed: 9122164]

Pugh CW, O'Rourke JF, Nagao M, Gleadle JM, Ratcliffe PJ. J Biol Chem. 1997; 272:11205–14. [PubMed: 9111021]

Rathmell WK, Chen S. Expert Rev Anticancer Ther. 2008; 8:63–73. [PubMed: 18095884]

Rathmell WK, Hickey MM, Bezman NA, Chmielecki CA, Carraway NC, Simon MC. Cancer Res. 2004; 64:8595–603. [PubMed: 15574766]

Sanchez-Elsner T, Botella LM, Velasco B, Langa C, Bernabeu C. J Biol Chem. 2002; 277:43799–808. [PubMed: 12228247]

Semenza GL. Nat Rev Cancer. 2003; 3:721–32. [PubMed: 13130303]

Semenza GL, Jiang BH, Leung SW, Passantino R, Concordet JP, Maire P, Giallongo A. J Biol Chem. 1996; 271:32529–37. [PubMed: 8955077]

Stebbins CE, Kaelin WG Jr. Pavletich NP. Science. 1999; 284:455–61. [PubMed: 10205047]

Tian H, McKnight SL, Russell DW. Genes Dev. 1997; 11:72–82. [PubMed: 9000051]

Voss AK, Thomas T, Gruss P. Development. 2000; 127:1–11. [PubMed: 10654595]

Williams-Simons L, Westphal H. Transgenic Res. 1999; 8:53–4. [PubMed: 10681148]

Zbar B, Kishida T, Chen F, Schmidt L, Maher ER, Richards FM, Crossey PA, Webster AR, Affara NA, Ferguson-Smith MA, Brauch H, Glavac D, Neumann HP, Tisherman S, Mulvihill JJ, Gross DJ, Shuin T, Whaley J, Seizinger B, Kley N, Olschwang S, Boisson C, Richard S, Lips CH, Lerman M, et al. Hum Mutat. 1996; 8:348–57. [PubMed: 8956040]

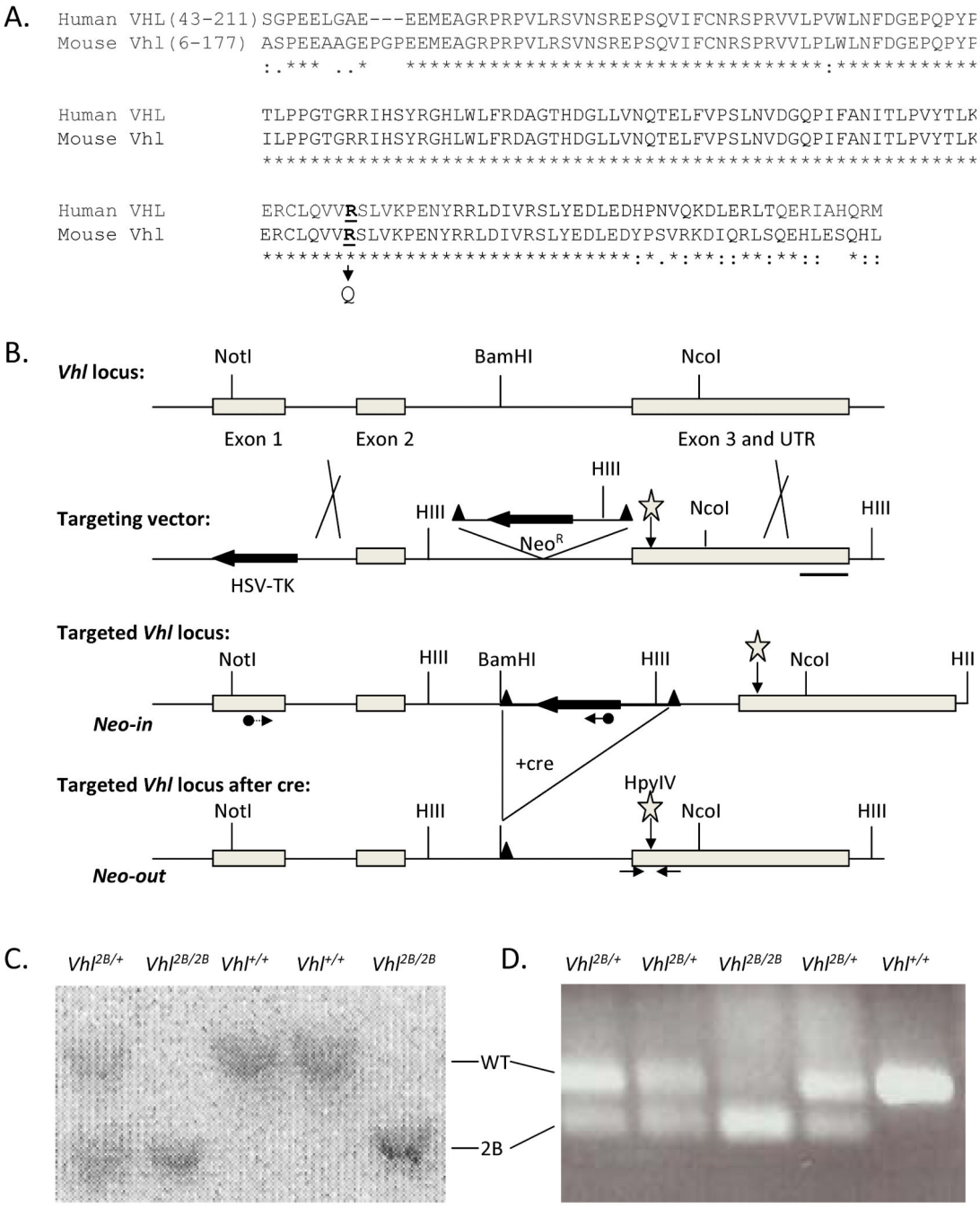

Figure 1.

Type 2B *Vhl* mutation knock-in strategy and genotyping. A. Human:Mouse pVHL protein alignment. The R167Q pVHL substitution representing human Type 2B VHL disease is embedded in a highly homologous region. B. Type 2B mutant murine *Vhl* containing the G518A (R167Q) representative missense mutation (star) was prepared with site-directed mutagenesis and then cloned into the targeting vector as shown. Following electroporation of the targeting vector into J1 ES cells, neomycin and gancyclovir resistance was used to select clones with homologous recombination at the endogenous murine locus (*Neo-in*). Cre

recombinase exposure *in vitro* or *in vivo* resulted in excision of the floxed Neo^R cassette (*Neo-out*). C. Southern blot genotyping distinguished between wild-type and targeted *Vhl* alleles based on the introduction of new HindIII restriction sites. HindIII-digested murine *Vhl* was detected with a probe recognizing the *Vhl* 3′ untranslated region (UTR, bar). D. Restriction PCR was used as an alternative genotyping strategy. Primers (arrows) flanking the targeted mutation generated a 300-bp PCR product. The novel restriction site introduced by the G518A mutation rendered the targeted *Vhl*-origin PCR product susceptible to HpyIV digestion.

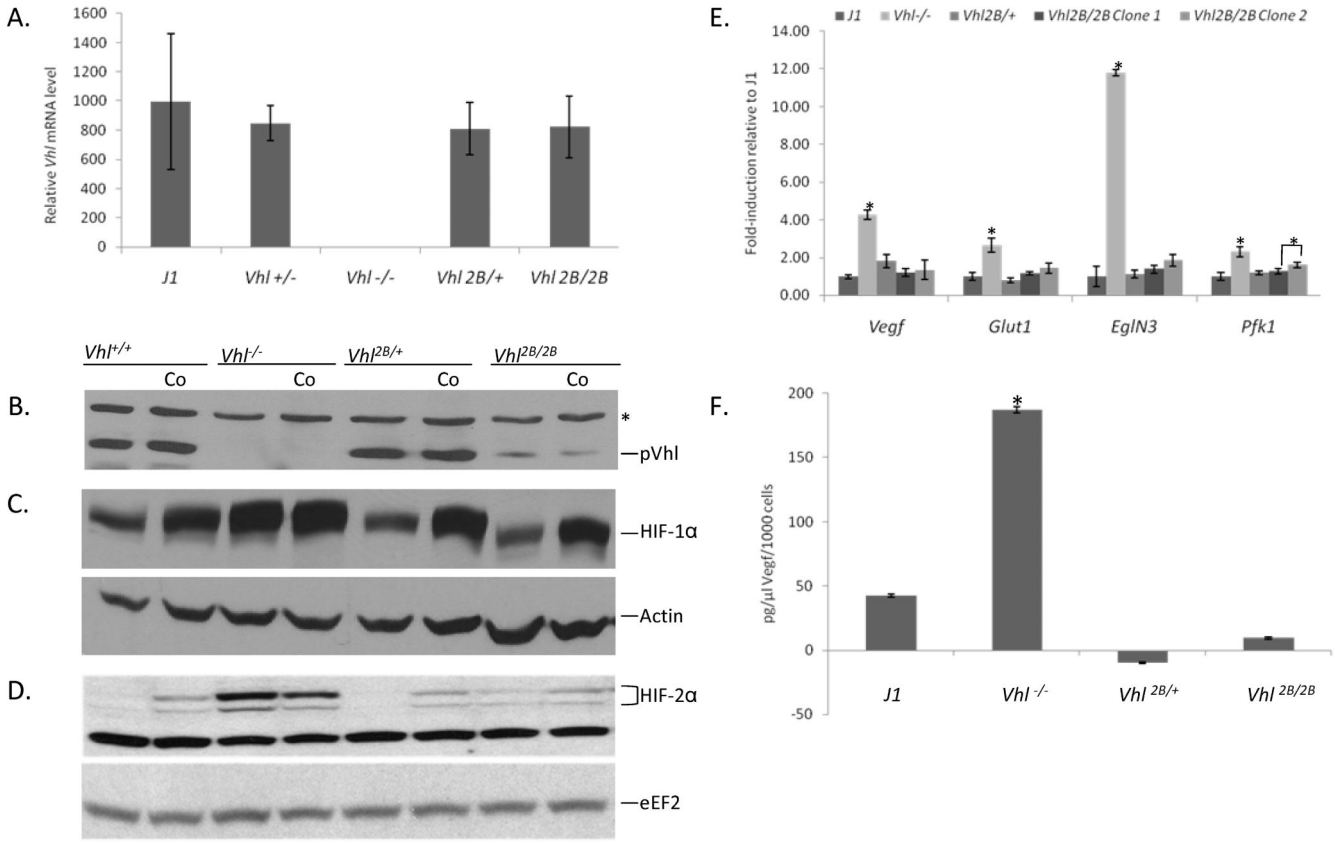

Figure 2.

The Type 2B *Vhl* missense mutation results in a post-transcriptional reduction in mutant pVHL levels and slight normoxic HIF dysregulation but normal normoxic suppression of HIF target gene transcription in ES cells. A. Quantitative RT-PCR analysis for *Vhl* cDNA levels in ES cells relative to expression of the wild-type allele. Quantitation was normalized to an internal *18S* ribosomal RNA standard. Error bars indicate standard error of the mean (SEM). B.-D. Immunoblots for pVhl (B.), HIF-1α (C.), and HIF-2α (D.) expression in ES cells treated with or without the hypoxia mimetic $CoCl_2$ (Co) for four hours. E. Quantitative RT-PCR for normoxic transcriptional activation of HIF targets *Vegf*, *Glut1*, *EglN3*, and *Pfk1* in ES cells relative to J1. Cycle thresholds were corrected with *18S* ribosomal RNA. Error bars indicate SEM. *$p<0.05$ in paired comparison to J1. ELISA for secreted Vegf protein in ES cells relative to J1. *$p<0.01$ in paired comparison to J1.

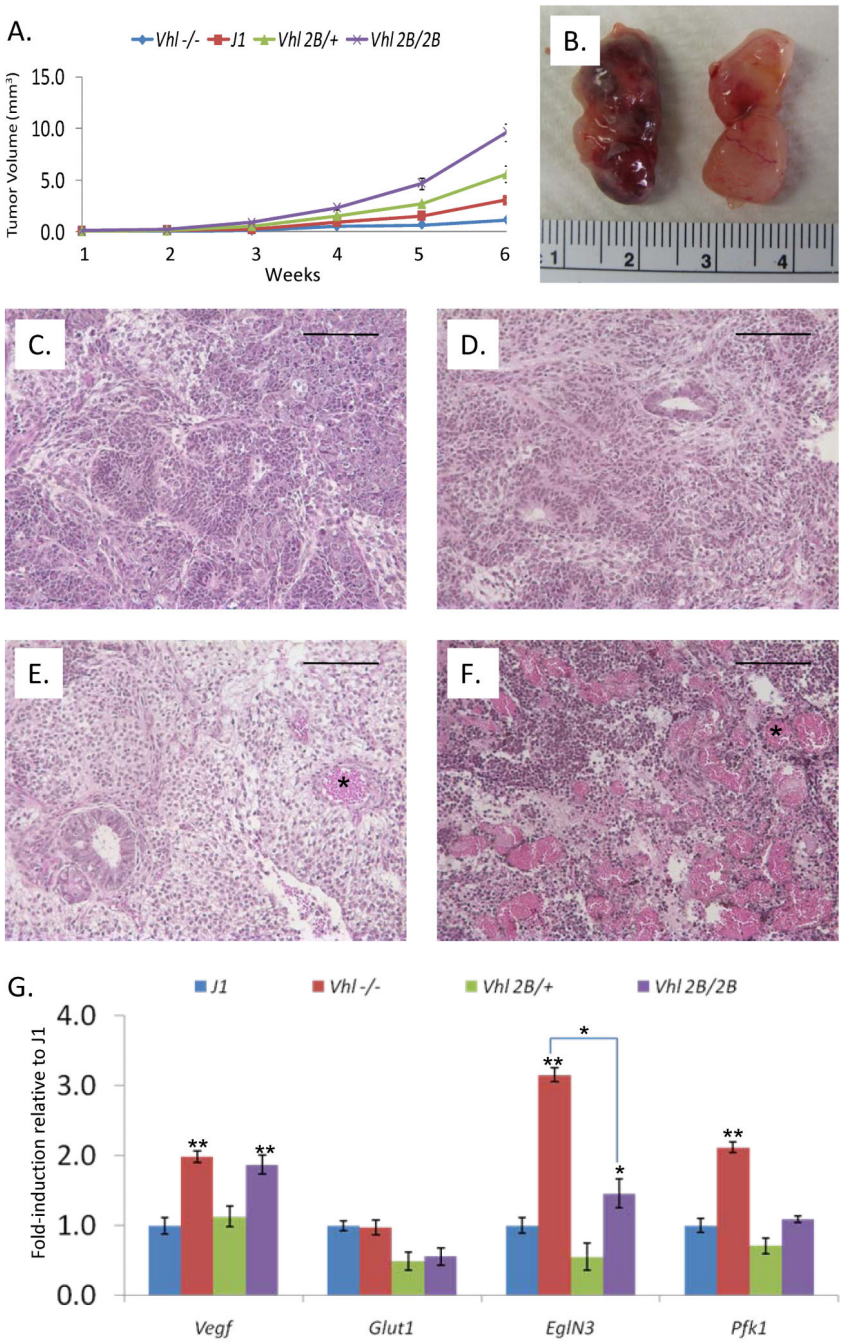

Figure 3.

Homozygous Type 2B *Vhl* teratomas display growth advantage, enhanced hemangioma formation, and transcriptional dysregulation of HIF target genes. A. Growth curve for ES cell-derived teratomas (n=6 per genotype). Error bars indicate SEM. B. Gross appearance of representative $Vhl^{2B/2B}$ (left) and $Vhl^{2B/+}$ teratomas. C.-F. Histological analysis of representative J1 (C.), $Vhl^{-/-}$ (D.), $Vhl^{2B/+}$ (E.), and $Vhl^{2B/2B}$ (F.) teratoma morphology by H&E at 20X magnification. Note enhanced hemangioma (*) formation and hemorrhage in $Vhl^{2B/2B}$ relative to $Vhl^{-/-}$ teratoma. Scale bars indicate 100μm. G. Quantitative RT-PCR for

transcriptional activation of HIF targets *Vegf*, *Glut1*, *EglN3*, and *Pfk1* in representative set of teratomas relative to J1. Cycle thresholds were corrected with *18S* ribosomal RNA. Error bars indicate standard deviation. *p<0.05. **p<0.001.

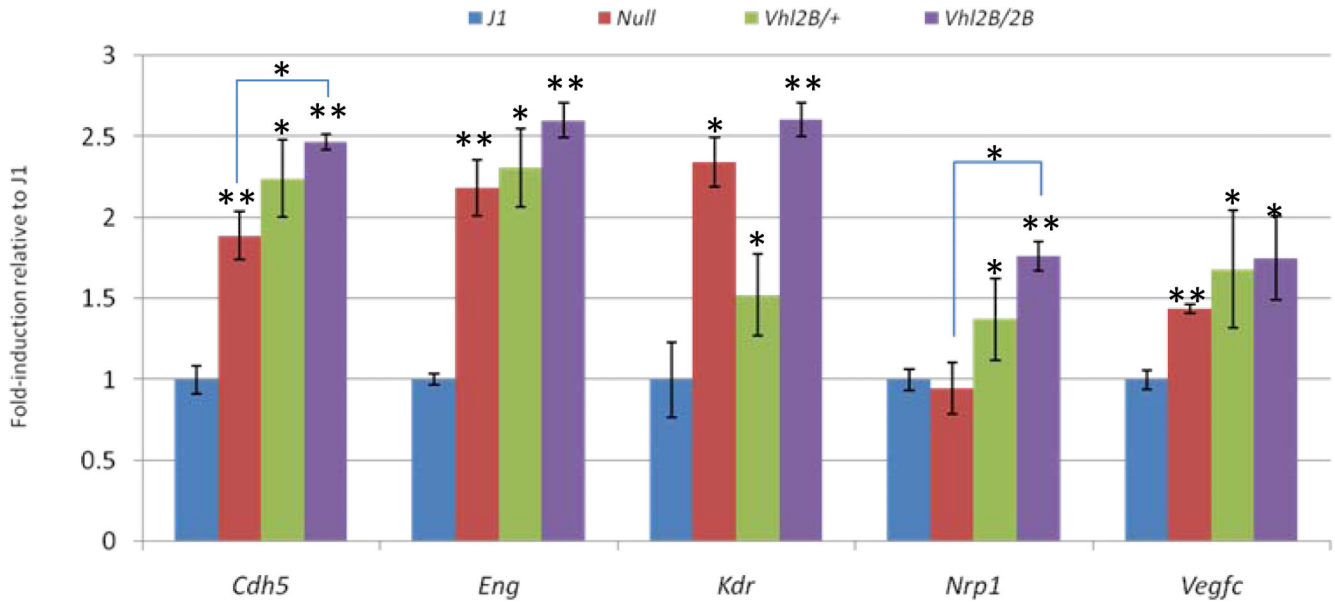

Figure 4.

Exploration of hyper-angiogenic phenotype of homozygous Type 2B *Vhl* teratomas. Quantitative RT-PCR for transcriptional activation of angiogenesis-related genes *Cdh5*, *Eng*, *Kdr*, *Nrp1*, and *Vegfc* in a representative set of teratomas relative to J1. Cycle thresholds were corrected with *18S* ribosomal RNA. Error bars indicate standard deviation. *p<0.05. **p<0.001.

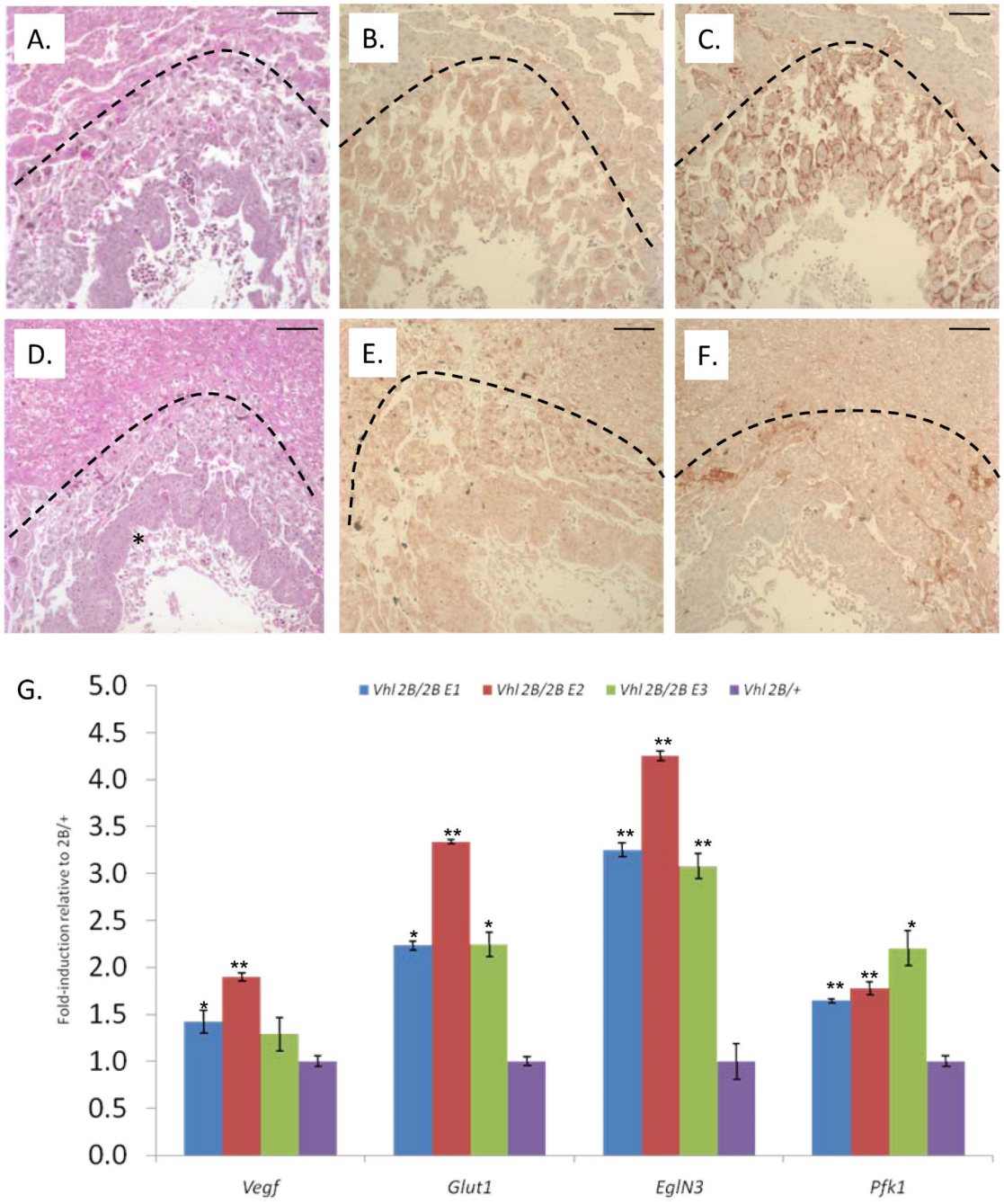

Figure 5.

Homozygous Type 2B *Vhl* placentas display subtle vascular defects consistent with a *Vhl*-null phenotype, and corresponding embryos display HIF target dysregulation despite normal morphology. A.-F. Histological analysis of $Vhl^{2B/+}$ (A.-C.) and $Vhl^{2B/2B}$ (D.-F.) murine placentas, with H&E stain for morphology (A., C.) and immunohistochemistry for pVhl (B., E.) and for the HIF target Vegfa (C., F.) at 10X magnification. Arcs demarcate the maternal decidua (above) and placental (below) tissues. Note the lack of nucleated fetal RBCs (*) in the chorionic villi in $Vhl^{2B/2B}$ (D.) versus $Vhl^{2B/+}$ (A.) placentas. Scale bars indicate 100μm.

G. Quantitative RT-PCR for transcriptional activation of HIF targets *Vegf*, *Glut1*, *EglN3*, and *Pfk1* in E9.5 $Vhl^{2B/2B}$ embryos relative to representative $Vhl^{2B/+}$ littermate. Cycle thresholds were corrected with *18S* ribosomal RNA. Error bars indicate SEM. *p<0.05. **p<0.001.

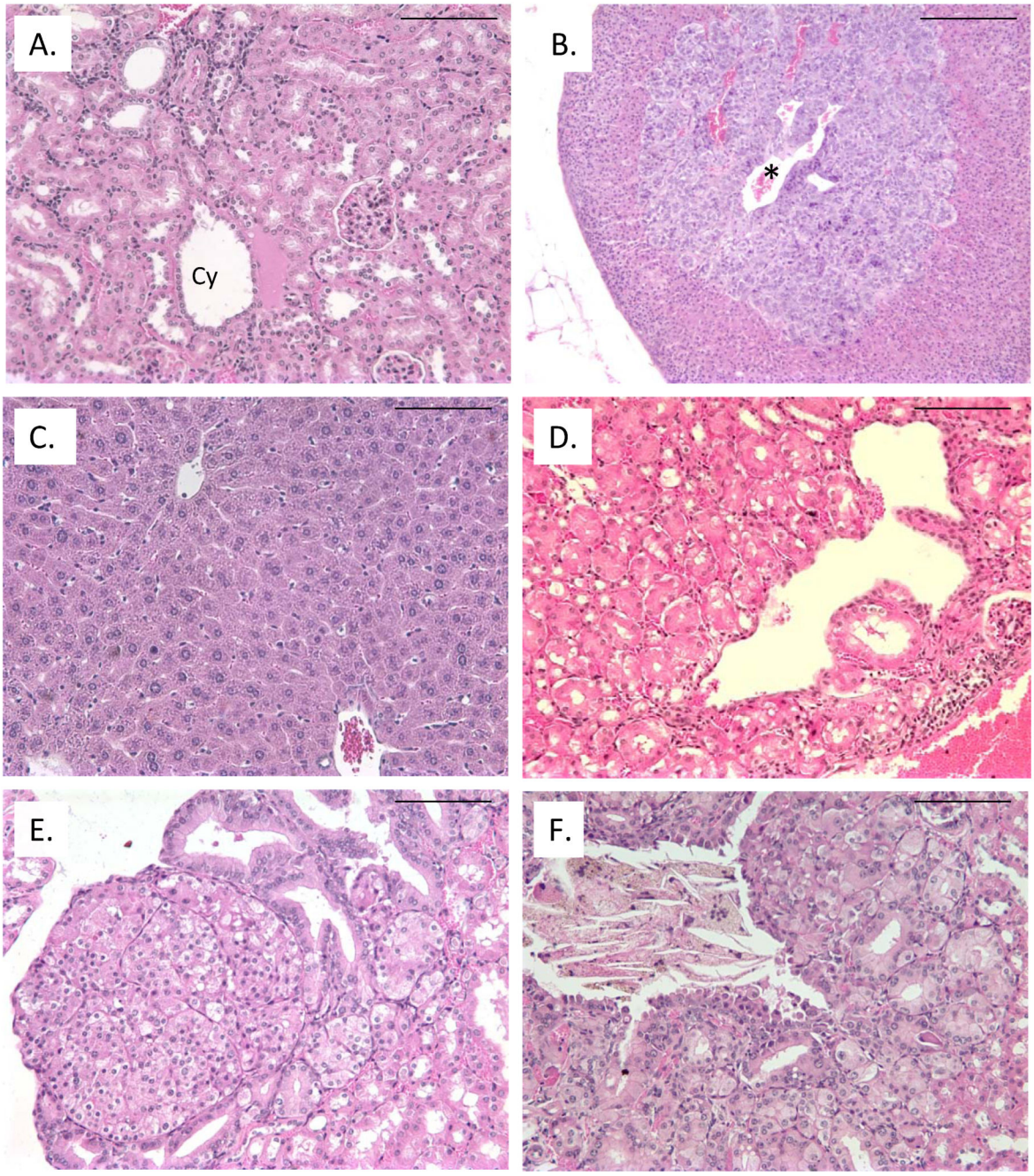

Figure 6.

Adult Type 2B *Vhl* heterozygous mice develop mild vascular lesions and rare renal cortical microcysts, while transplacental ENU mutagenesis reveals renal tumor predisposition. A. - D. Histological analysis of representative adult Type $Vhl^{2B/+}$ mouse tissues, including kidney (A.), adrenal gland (B.), and liver (C.) by H&E stain at 20X magnification. $Vhl^{2B/+}$ mice frequently developed renal (not shown) and adrenal (B., *) angiectasis and occasionally developed simple renal cortical microcysts (A., Cy). E. - F. Histological analysis of ENU-mutagenized $Vhl^{2B/+}$ mice by H&E stain at 20X magnification. While ENU

mutagenesis promoted benign simple and papillary microcysts formation in both *Vhl*$^{2B/+}$ (not shown) and wild-type littermates (D.), borderline adenoma/adenocarcinoma (E.) and adenocarcinoma (F.) were selectively observed in mutagenized *Vhl*$^{2B/+}$ mice at twelve months. Scale bars indicate 100μm.

Table 1

Vhl genotype analysis of inter-heterozygous matings at birth and embryonic time points

Vhl	**E9.5**	**E10.5**	**Birth**
+/+	14 (32%)	13 (45%)	60 (36%)
2B/+	20 (49%)	15 (52%)	107 (64%)
2B/2B	8 (19%)	1 (3%)	0 (0%)
Total	42	29	167

Table 2

Summary of renal lesions observed in ENU-mutagenized *Vhl*$^{2B/+}$ and wild-type littermates

	4 months		12 months	
	Vhl $^{+/+}$ **(n=4)**	***Vhl*** $^{2B/+}$ **(n=8)**	***Vhl*** $^{+/+}$ **(n=14)**	***Vhl*** $^{2B/+}$ **(n=10)**
Renal Microcyst(s)	3	6	11	7
-Papillary	3	1	2	1
Pre-neoplasia	0	1	0	0
Neoplasia	0	0	0	2